# Lipid Structural Effects of Oral Administration of Methylphenidate in *Drosophila* Brain by Secondary Ion Mass Spectrometry Imaging

Nhu T. N. Phan,[†,‡] John S. Fletcher,[†,‡,§] and Andrew G. Ewing*,[†,‡,§]

[†]Department of Chemistry and Molecular Biology, University of Gothenburg, Kemivägen 10, SE-412 96 Gothenburg, Sweden
[‡]National Center Imaging Mass Spectrometry, Kemivägen 10, SE-412 96 Gothenburg, Sweden
[§]Department of Chemistry and Chemical Engineering, Chalmers University of Technology, Kemivägen 10, SE-412 96 Gothenburg, Sweden

ⓢ *Supporting Information*

ABSTRACT: We use time-of-flight secondary ion mass spectrometry (TOF-SIMS) imaging to investigate the effects of orally administrated methylphenidate on lipids in the brain of *Drosophila melanogaster* (fruit fly), a major invertebrate model system in biological study and neuroscience. TOF-SIMS imaging was carried out using a recently designed high energy 40 keV Ar_{4000}^+ gas cluster ion gun which demonstrated improved sensitivity for intact lipids in the fly brain compared to the 40 keV C_{60}^+ primary ion gun. In addition, correlation of TOF-SIMS and SEM imaging on the same fly brain showed that there is specific localization that is related to biological functions of various biomolecules. Different lipids distribute in different parts of the brain, central brain, optical lobes, and proboscis, depending on the length of the carbon chain and saturation level of fatty acid (FA) branches. Furthermore, data analysis using image principal components analysis (PCA) showed that methylphenidate dramatically affected both the distribution and abundance of lipids and their derivatives, particularly fatty acids, diacylglycerides, phosphatidylcholine, phosphatidylethanolamine, and phosphatidylinositol in the fly brains. Our approach using TOF-SIMS imaging successfully visualizes the effects of methylphenidate on the chemical structure of the fly brain.
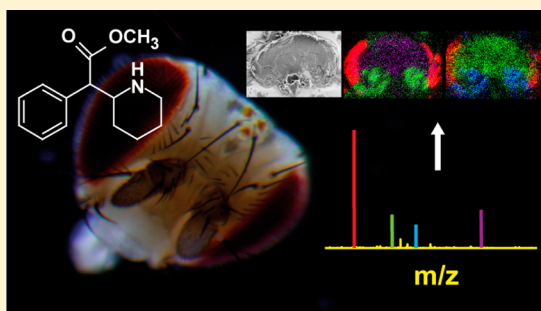
Methylphenidate (MPH), an effective treatment for attention deficit/hyperactivity disorder (ADHD) in children and adolescents, has been shown to elicit psychostimulant effects and addiction similar to cocaine and amphetamine.[1,2] Because of a similar chemical structure to cocaine and amphetamine, MPH can block the reuptake by neurotransmitter transporters leading to the elevated synaptic catecholamine neurotransmitters in the brain, which causes a euphoric feeling and addiction in long-term use. Despite the widespread use as a therapeutic drug, the mechanisms of action of MPH on the nervous system are not clearly understood. A rising concern about the long-term treatment of MPH involves the adverse effects on the neurotransmitter system and the structure and function of the brain. It was shown that the levels of neurotransmitters and metabolites in *Drosophila* brain were dose dependent following administered MPH, and these were saturated at the administration dose of 20−25 mM.[3] There is also evidence that in addition to acting on the catecholamine systems, MPH induces significant changes in the lipid composition of the brain,[4] blood,[5] and plasma.[6] However, detailed information about specific kinds of lipids as well as spatial distributions of the target molecules affected by the drug has not been provided.

Being one of the most common model systems in biological and neurological studies, *Drosophila melanogaster* (fruit fly) is

an ideal model for the study of mechanisms of drug abuse and neurological disorders such as epilepsy, Niemann-Pick disease, and Parkinson's disease.[7−10] *Drosophila* has been used in fast scan cyclic voltammetry studies of the blocking efficiency of orally administrated MPH on dopamine uptake and its effects on cocaine action on dopamine transporters.[11] Kliman and co-workers applied highly selective and sensitive mass spectrometry (MS) coupled with ion mobility spectrometry to analyze the lipid profile in *Drosophila* epilepsy brains.[10] Another example was the use of *Drosophila* for proteomic profiling for Parkinson's disease using multidimensional liquid chromatography coupled with MS.[12]

Mass spectrometric imaging (MSI) techniques have recently attracted increasing interest in different research areas especially biology, pharmaceuticals, and neuroscience. MSI provides the opportunity to obtain the spatial structure of various biomolecules in many biological bodies from single cells to large biological tissue sections of several centimeters. Despite having a body of less than 2 mm and a head less than 1 mm in length, *Drosophila* has also been an attractive model for this new imaging area. *Drosophila* was used to study the distribution

of six lipid classes including phosphatidylcholines, phosphatidylethanolamines, phosphatidylinositols, phosphatidylserines, and triacylglycerides in the entire body of the fly[13] and to study the phospholipid distribution in the submillimeter-sized egg chamber using matrix assisted laser desorption ionization imaging mass spectrometry (MALDI-MSI).[14] We have developed an imaging protocol using time-of-flight secondary ion mass spectrometry (TOF-SIMS) for *Drosophila*, aimed at studying lipids and lipid related compounds in the fly brain with 3 μm spatial resolution.[15]

In a range of MSI techniques, TOF-SIMS is one of the most favorable in many different application areas. TOF-SIMS imaging has been increasingly used in biological applications owing to not only its nontargeted approach and chemical specificity like other MSI techniques but also its superior spatial resolution (<5 μm) and label or matrix-free sample preparation. The technique is best suited for detection of small molecules, intact lipids, and small peptides with m/z < 1500 Da. To perform TOF-SIMS imaging, a primary ion beam is used to sputter the sample surface to produce secondary ions, which then travel through the mass spectrometer to be separated and detected by their difference in m/z.

Various primary ion guns have been developed for SIMS in order to improve spatial resolution, sensitivity, and to expand the capability to detect larger molecules.[16−19] Gas cluster ion beams (GCIB) have been widely used as the etching beam for depth profiling in SIMS. The beams show low subsurface damage and remarkably reduced fragmentation of the secondary ions due to softer sputtering by the clusters.[20,21] This leads to improved signal levels of large molecules such as lipids and small peptides compared to liquid metal ion guns (Au$_3$, Bi$_3$) and polyatomic ion guns (C$_{60}$). GCIBs therefore have been utilized as analysis beam. A water cluster ion gun 10 keV (H$_2$O)$_{1000}$$^+$ has been developed by the Vickerman group to increase the ion yield by enhanced proton mediated reaction.[22] The gun showed 10 times improvement in the ion yield when applied to lipid standard samples. More recently, Angerer et al. compared the performance between the 40 keV C$_{60}$$^+$, 20 keV Ar$_{4000}$$^+$, and new high energy 40 keV Ar$_{4000}$$^+$ guns on brain tissues and human hair samples.[23] The results showed that the 40 keV Ar$_{4000}$$^+$ produced the highest signals (secondary ion yield) relative to the other guns when the m/z was above 500 and a spatial resolution of <3 μm was obtained. GCIBs have been shown to provide great potential as analysis beams for imaging lipid and lipid related compounds in biological samples.

In this paper, we apply SIMS imaging using the 40 keV Ar$_{4000}$$^+$ GCIB to study the distribution of biomolecules in *Drosophila* brain and to determine how specific lipids are affected by the oral administration of MPH. We also use SEM imaging as a correlation tool with SIMS imaging in order to relate the chemical and morphological structure of the brain. This is useful for understanding the relation between the biomolecular distribution and brain function.

■ EXPERIMENTAL SECTION

Fly Culture and Sample Preparation for SIMS Imaging. Transgenic *Drosophila* flies (TH-GFP) were cultured on potato meal/agar medium. Detailed fly culturing protocols for the methylphenidate (MPH) treated and control flies can be found in previous literature.[3,24] After culture, the live drug treated and control flies were then alternatively loaded into a fly collar (4 M Instrument & Tool LLC), which kept all the fly

heads in the same orientation. In order to subsequently obtain good sectioning, the fly collar contained no more than 11 flies. The fly collar was then put into a mold filled with 10% gelatin (Sigma-Aldrich, Stockholm, Sweden), which subsequently was solidified and frozen at −20 °C. The frozen gelatin block containing the fly heads was detached from the fly collar and sectioned using a cryo-microtome (Leica CM 1520, Leica Biosystems) at −20 °C under argon atmosphere to produce slices of 20-μm thickness in the dorsal direction. The brain sections were placed onto indium tin oxide (ITO) coated microscope slides and transported under liquid nitrogen to an argon-filled glovebox on the *J105* SIMS instrument (Ionoptika Ltd., U.K.). The sample was quickly mounted onto the precooled insertion stage of the instrument in argon atmosphere in the glovebox preventing water condensation on the sample surface. Finally, the frozen hydrated sample was transferred into the main chamber and the analysis was carried out at a temperature below −170 °C.

TOF-SIMS Imaging. TOF-SIMS measurements were carried out using a *J105* TOF-SIMS instrument, for which operation principles are described in more detail elsewhere.[25,26] The instrument is equipped with a 40 keV C$_{60}$$^+$ primary ion gun and a 40 keV Ar GCIB, which can produce clusters Ar$_{1000−4000}$. The measurements with Ar GCIB were performed statically in positive and negative modes with Ar$_{4000}$$^+$ containing 8% CO$_2$ to improve cluster formation. The focus of the ion beam was adjusted using different apertures. The beam size 6 μm/pixel with the primary ion current 50 pA was used to acquire the images of 128 × 128 pixels. The resulting primary ion dose density was approximately 5.6 × 10^{12} ion/cm^2. Higher resolution images with 256 × 256 pixels were obtained with the beam size of 3 μm/pixel which produced a current of 9 pA and a primary ion dose density of 4.0 × 10^{12} ion/cm^2. The measurement with the 40 keV C$_{60}$$^+$ gun was performed with 10 pA primary current and 1 μm/pixel beam size to obtain image of 256 × 256 pixels. The corresponding ion dose density was 3.8 × 10^{12} ion/cm^2. The instrument provided mass resolution ($m/\Delta m$) of ∼6000 for m/z 798.64. For frozen hydrated analysis, the insertion stage and the analysis chamber were cooled down to −178 °C before the sample was inserted. During the measurement, the analysis chamber was kept below −170 °C.

Data Analysis. TOF-SIMS data were processed using Image Analysis Software developed by Ionoptika Ltd. Data can be transformed to different formats suitable for further analysis, particularly principal components analysis (PCA). PCA analysis was carried out using Matlab (version R2013a, TheMathWorks). To reduce the number of data points and, hence, memory requirements, the spectra were binned to 0.05 m/z unit bins, which resulted in the mass accuracy 62 ppm at m/z 800. The spectra were then filtered from the background peaks (peaks from ITO coated glass and gelatin embedding material), mean centered, and normalized to the number of pixels of the analysis area and total ion counts of selected peaks before PCA analysis with NIPALS algorithm. Following PCA analysis, peak assignment was carried out using the unbinned data, which has a mass accuracy of about 6 ppm at m/z 800.

■ RESULTS AND DISCUSSION

TOF-SIMS Imaging of the Fly Brain with the Gas Cluster Ion Beam (GCIB). The intensities of high mass ions are significantly improved when analyzed following ionization with the GCIB owing to soft sputtering of the sample surface,

which gives less fragmentation for the ionized species. Generally GCIBs, particularly the Ar clusters with low energy (often 10 keV), have been used as etching beams. In our experiment, a unique high energy 40 keV Ar GCIB has been used as the analysis gun. The high energy of the gun makes it easier to focus the beam, with spot sizes as small as 2 μm possible. In addition, large clusters (Ar_{4000}) can be produced reducing the energy of individual Ar atoms in order to impact the surface molecules more gently.

To demonstrate the advantageous performance of the GCIB regarding sensitivity for high mass species, comparison of the chemical distribution and mass spectra of the fly brain was performed between the 40 keV Ar_{4000}^{+} and the 40 keV C_{60}^{+} beam. From the ion images (Figure 1A), small molecules such
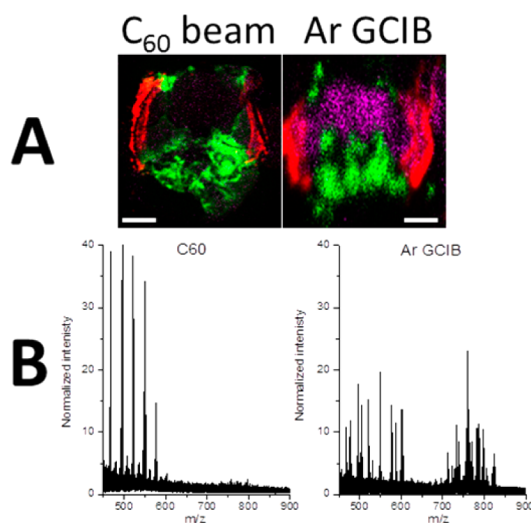

Figure 1. Improved signals of intact lipids in the fly brain obtained by 40 keV Ar_{4000} GCIB compared to 40 keV C_{60} ion beam. (A) Biomolecular distribution in the fly brains. Drosopterin at m/z 369.16 (red), DAG (30:1) at m/z 521.47, DAG (32:1) m/z 549.53 (green), lipids PC (32:1) m/z 732.61, PC (34:1) m/z 760.65 (purple). (B) Signal intensities of DAGs and intact lipids. Scale bar is 200 μm.

as the eye pigment Drosopterin at m/z 369.16 and different diacylglycerides (DAGs), for example, DAG (30:1) at m/z 521.47, DAG (32:1) at m/z 549.53 are detected with high intensities when both primary ion guns are used. Both images are consistent in regional distribution of detected ions. The intact lipid signals such as phosphatidylcholine (PC) (32:1) at m/z 732.61 and PC (34:1) at m/z 760.65 are clearly observed when analyzed using the Ar_{4000} GCIB, whereas they are hardly detected when the C_{60} gun is used. Whereas the GCIB allows us to detect these higher masses that are difficult to see with C_{60}, even with the GCIB the relatively weak signal compared to that for lower masses makes the image slightly grainy. With equivalent primary ion dose, the ion image obtained when the Ar_{4000} GCIB is used is not as good as that with the C_{60} gun owing to a less focused beam (1 μm beam size for C_{60} gun); however, this still provides a very clear distributional structure of different molecules in a fly brain, which is less than 1 mm in size. The corresponding spectra (Figure 1B) show that within the low mass range below m/z 700, the peak intensities obtained by both guns are in a similar range; however, for mass range above m/z 700, peak signals obtained with the Ar_{4000} GCIB are significantly higher than those when the C_{60} gun is used.

Tremendous improvement in the sensitivity for detection of intact lipids with the 40 keV Ar_{4000}^{+} GCIB over the 40 keV C_{60}^{+} beam are clearly shown with a small trade off in imaging resolution, which is useful for the scope of study presented here in terms of brain size. The Ar_{4000} GCIB, therefore, was used for further fly brain investigation.

Chemical and Morphological Structure of the Fly Brain Using Multimodal SIMS and SEM Imaging. Multimodal imaging is a common approach in biological studies where the chemical structure of a sample is correlated with its morphological features in order to gain more understanding about the sample, especially the distribution of different biomolecules in relation to their biological functions in specific regions of the sample. From the ion images of the fly brain, a number of biomolecules show various differing localizations in the brain, thus correlation between SIMS and scanning electron microscopy (SEM) imaging is very useful for the data interpretation. The same fly brain sample was prepared for imaging with SIMS and subsequently with SEM. The sample was kept frozen-hydrated for SIMS imaging and then was freeze-dried for SEM. It has been reported that frozen-hydrated sample preparation better preserves the chemical structure of the fly brain than freeze-drying.[15] This might result from chemical migration during the drying process for the freeze-drying method; therefore, the frozen-hydrated preparation has been preferentially used here. After the TOF-SIMS experiment, the sample was slowly freeze-dried overnight in the sample preparation chamber of the J105 where the vacuum was about 10^{-5} mbar and then stored for analysis with SEM.

The SIMS and SEM images are compared in Figure 2. The morphological structure of the dorsal surface of the fly brain section is well maintained as shown in Figure 2A. The brain has three main regions: central brain, two symmetric optical lobes on two sides, and the proboscis at the bottom. Images of each region are shown with higher magnification to elucidate more structural detail (Figure 2B–D). The central brain exhibits very smooth surface features except several cracking lines, which are assumed to have occurred during the drying process and storage before analysis.

In the optical lobes (Figure 2C), a very complicated structure is observed with the compound eye (ommatidia) arranged in a very delicate pattern in the outermost surface to receive light from the surroundings. Underneath the compound eye are numerous eye pigments, which are incorporated deep into the optical lobes in order to transfer the visual signals from the compound eye to the optical lobes. The area nearby the proboscis, on the other hand, has a rough surface containing a number of holes (Figure 2D). This is the salivary gland area, thus the holes are from the tube shaped structure of the glands. Different regions have specific morphological features that can be easily distinguished. TOF-SIMS ion images obtained in positive ion mode (Figure 2E,F) show that distributions of different biomolecules are significantly different across the brain. Figure 2A,E are the same size and orientation for the same brain and therefore can be overlaid as shown in Figure S1 in the Supporting Information. The previously identified eye pigment, a Drosopterin[15] $[C_{15}H_{16}O_2N_{10} + H]^{+}$ at m/z 369.16 localizes in the optical lobes as expected. Several diacylglycerides (DAGs), particularly DAG (26:0) at m/z 467.43, DAG (28:0) at m/z 495.46, DAG (30:1), and DAG (32:1) are distributed in the cuticle and salivary gland areas. DAGs might be part of the chemical composition of the cuticle and also the salivary fluid; therefore, these are observed in Figure 2E at the
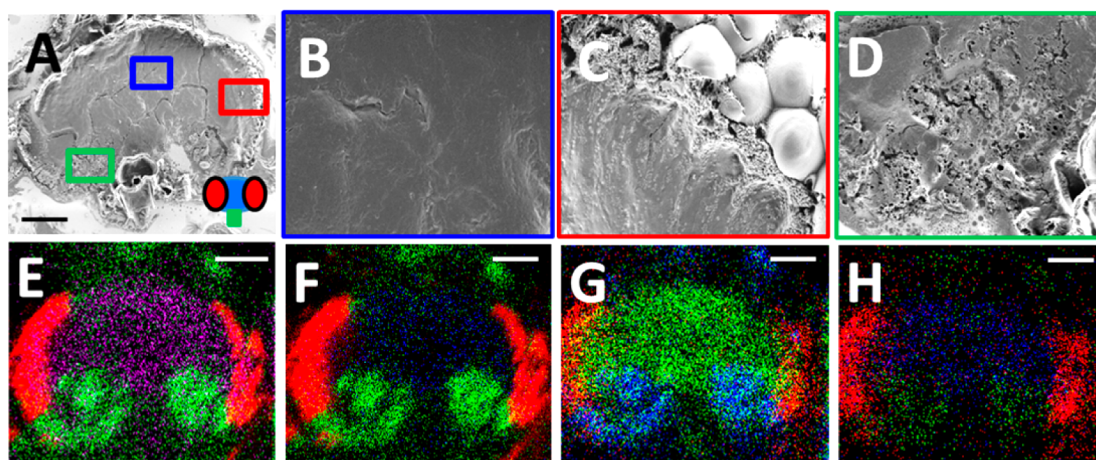
Figure 2. Chemical structure of a fly brain using multimodal SIMS and SEM imaging. (A) SEM image of a fly brain section. Symbolic figure on the right bottom shows the orientation of the fly brain, two red parts on the side are optical lobes, the central brain is the middle (blue), and the lower part is proboscis (green). (B) Zoom-in image of the central brain. (C) Zoom-in image of eyes. (D) Zoom-in image of salivary gland area. (E, F) SIMS ion image in positive ion mode; (E) Drosopterin m/z 369.16 (red), DAG (30:1) m/z 521.47, DAG (32:1) m/z 549.53 (green), lipids PC (32:1) m/z 732.61, PC (34:1) m/z 760.65 (purple); (F) Drosopterin m/z 369.16 (red), DAG (26:0) m/z 467.43, DAG (28:0) m/z 495.46 (green), lipid PC (36:2) m/z 786.64 (blue). (G, H) SIMS ion image in negative ion mode; (G) Drosopterin m/z 368.08 (red), fatty acid (C18:1) m/z 281.21 (green), fatty acid (C14:0) m/z 227.18 (blue); (H) Drosopterin m/z 368.08 (red), PI (32:1) m/z 807.47 (green), PE (36:3) m/z 740.55 (blue). Scale bar is 200 μm.

openings caused during sectioning of the glands in the fly brain and shown in Figure 2D. As the DAGs are part of the composition of the fluid, this leads to smearing and migration of these molecules during sample preparation and this could explain why, when samples are analyzed at room temperature, DAGs distribute over the entire brain. The intact lipids mainly phosphatidylcholines (PCs), on the other hand, were found to mainly localize in the central brain area such as PC (32:1), PC (34:1), PC (36:2) at m/z 786.61 as well as their salt adducts, for instance $[PC\ (36:2) + K]^+$ at m/z 824.57. PCs are the main component of the outer leaflet of the plasma membrane facilitating the membrane trafficking, integration of membrane proteins.[27,28] PCs are an important reservoir for secondary messengers such as diacylglycerol, phosphatidic acid, and arachidonic acid, which regulate different physiological cellular functions particularly cell death, proliferation, and differentiation.[29−31] Moreover, PCs as well as other lipids also play important roles in brain functions because various brain injury and degradative neurological diseases such as cerebral ischemia, stroke, schizophrenia, and Alzheimer's disease have been found to show related perturbation of PCs.[32,33] In the rat brain, PCs localize in specific regions, for instance the gray matter and white matter regions, the hippocampus, and cerebral cortex, striatum and corpus callosum depending on their fatty acid chains and saturation levels. The properties of the fatty acid chains in PCs influence the fluidity, curvature, and functions of the membrane.[34,35] PC (32:0) at m/z 734.65 and PC (34:1) were observed enriched in the gray matter regions especially in olfactory bulb, piriform cortex, and cerebellum whereas PC (36:1) distributed evenly in both gray and white matter areas of the rat brain.[36,37]

The negative ion mode was used to examine the distribution of different groups of molecules, especially fatty acids, phosphatidylethanolamine, and phosphatidylinositol lipids. Figure 2G shows the distribution of the eye pigment, Drosopterin $[C_{15}H_{16}O_2N_{10}]^-$ at m/z 368.08 and is consistent with its distribution observed in positive mode. Strong signals for fatty acids are observed. Interestingly, fatty acid (C18:1) at

m/z 281.21 localizes in the central brain, whereas fatty acid (C14:0) at m/z 227.18 is distributed in the cuticle and salivary gland areas. Other fatty acids found predominantly in central brain are (16:0) at m/z 255.20, (C18:3) at m/z 277.19, (C18:2) at m/z 279.22, and those in the cuticles are (C12:0) at m/z 199.15. Fatty acids localize differently in the brain depending on their carbon chain and saturation level. In addition, correlation of the ion images of positive and negative modes shows that fatty acids of C18, fatty acid of saturated C16, and PCs localize in the central brain, therefore those fatty acids could be the fragments from the carbon chains of PCs. On the other hand, the fatty acids of saturated C12, saturated C14, and DAGs all have similar localization in the cuticle and salivary gland area. These might be from intact phospholipids but are likely the fragments from triacylglycerides (TAGs). TAGs are known to be a major component of the insects cuticle, which helps make the cuticle waterproof and prevents transpiration.[13,38,39] It is also commonly known as the major constituent of lipid droplets and fat tissues; therefore, TAGs could be a constituent of the oily salivary fluid in the salivary area.

The distributions of phosphatidylethanolamine (PE) and phosphatidylinositol (PI) are shown in Figure 2H. Signals obtained for PEs and PIs are lower in intensity compared to those of fatty acids. PI (32:1) at m/z 807.47 localizes to the cuticle and salivary gland areas, whereas PE (36:3) at m/z 740.55 localizes in the central brain. Other species also found in the central brain are PE (36:2) at m/z 742.57, PI (34:2) at m/z 833.50, PI (36:4) at m/z 857.55, and PI (36:3) at m/z 859.56. PEs are the second most abundant phospholipid class after PCs and are enriched in the inner leaflet of plasma membrane. Because of their conical shape, PEs play a very important role in regulating membrane curvature and membrane protein activities.[40] PEs comprise about 45% of the total phospholipids in mammalian brain.[41] Moreover, they are the main precursors for the synthesis of ligands for cannabinoid receptors in the brain and glycosylphosphatidylinositol anchors, which help membrane proteins attach to the plasma membrane. PIs on the

other hand constitute less than 1% of the total membrane lipids. Their biological functions, however, are very important in cellular signaling regulating different cellular processes such as cell division, secretion, and motility.[42] Besides, PIs together with their phosphorylated PIs are the main sources for secondary messengers and influence different protein functions for example phospholipases, protein kinases, calcium ion channels.[31] PIs have been found to distinctly distribute in the gray matter of the freeze-dried mouse brain when analyzed by TOF SIMS with a Bi_3^+ primary ion gun.[43,44] Niehoff et al.[13] found nine species of PIs in *Drosophila* using MALDI imaging, especially PI (36:3), which was shown to be abundant in the hindgut and in the brain. Interestingly, we did not observe any peaks from lysolipids in the fly brain with our experimental conditions.

It is clear that the spatial distribution of different molecules in the fly brain relates closely to their biological function. We show that multimodal SIMS and SEM imaging is a very useful approach to explore the complex structure of these biological samples.

Oral Administration of Methylphenidate Affects the Chemical Structure of the Fly Brain Investigated by Image Principal Components Analysis (PCA). Multivariate analysis especially principal components analysis (PCA) is a very useful data analysis tool for many applications in TOF-SIMS such as for identification of biomarkers associated with specific diseases in biological samples, classification of chemicals, or sample groups in a data set.[45,46] PCA can be applied for both TOF-SIMS mass spectra and ion images. For mass spectra, PCA identifies the variance between groups of spectra based on the signal intensities of different m/z values. For ion images, PCA visualizes the variance between pixels, and each pixel produces one spectrum, based on the signal intensities of different m/z values in the spectra. More details of the image PCA method have been presented in a previous study.[15] Here, image PCA has been used to observe the distributional changes of biomolecules across the fly brain caused by the drug methylphenidate.

Images of control and MPH-treated brains were obtained by TOF-SIMS imaging with the Ar_{4000} GCIB and then combined together for image PCA analysis to obtain the same principal components for all images. Figure 3 compares the molecular distribution between control and MPH-treated brains using image PCA. In positive ion mode within the mass range of m/z 184−950, the significant differences are shown by principal component 2, by which phosphocholine headgroup at m/z 184.07, the eye pigment at m/z 369.16, pigment fragments at m/z 230.13, 231.14, and masses m/z 370.23, 407.20 localize in the optical lobes and central brain of the control brain, whereas those masses are only observed in the optical lobes of the MPH-treated brain. On the other hand, DAGs particularly DAG (30:1), DAG (32:1), DAG (28:0), DAG (26:0) at m/z 467.43, and DAG (34:1) at m/z 577.54 localize in the salivary and proboscis in both control and MPH treated brains. Another significant difference is noted in principal component 7. DAG (26:0), DAG (30:1), DAG (32:1), lipid PC (32:1), PC (34:1), PC (34:0) at m/z 758.60, and unknown species at m/z 439.42, 285.30, 211.24, 311.31, 218.15, 704.64 distribute in the optical lobes and proboscis but have different patterns between control and MPH treated brains. The eye pigment, Drosopterin, and unknown species at m/z 245.83, 246.83, 250.84, 376.78 distribute in the rest of the optical lobes and proboscis. In negative mode, principal component 3 shows fatty acids (14:0),
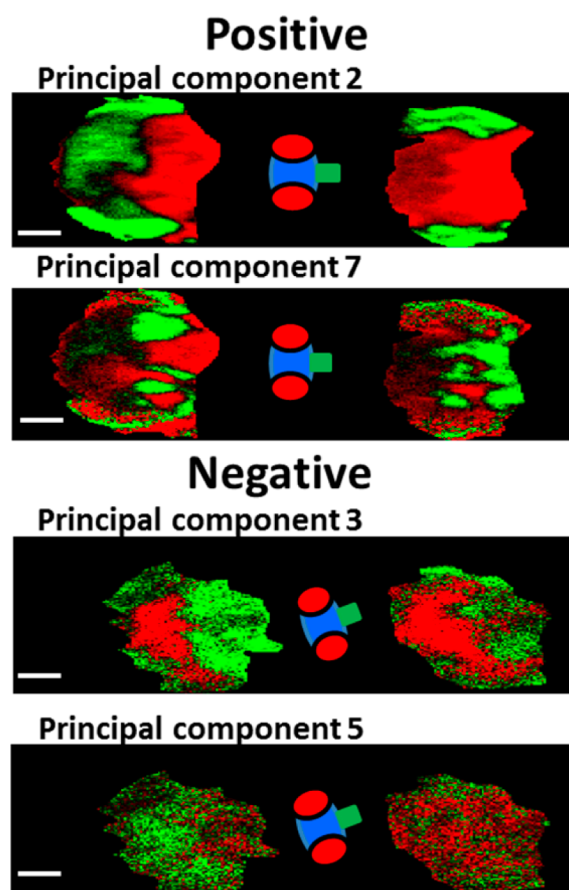

Figure 3. Image PCA to compare molecular distribution on MPH treated and control fly brains analyzed by 40 keV Ar_{4000} GCIB in positive ion mode and negative ion mode. Left, control brains; right, MPH treated brains. The symbolic figure shows orientation of the fly brains as per Figure 2. In positive mode, principal component 2: 369.16, 184.07, 230.13, 231.14, 218.15, 216.12, 370.23, 371.20, 407.20 are in the green area while DAGs at m/z 549.53, 521.47, 495.46, 467.43, 577.54 are in the red area. Principal component 7: DAGs at m/z 467.43, 495.46, 521.47, 549.53, 439.42, 285.30, 211.24, 311.31, 218.15, 730.69, 732.61, 758.60, 760.65, 768.61, 704.64 are in the green area while 369.16, 245.83, 246.83, 250.84, 376.78 are in the red area. In negative mode, principal component 3: 253.22, 227.18, 199.15, 166.99, 255.20 are in the green area while 281.21, 283.22, 277.19, 279.22, 260.86, 687.49, 659.43, 716.34, 726.50, 740.55, 742.48, 857.55 are in the red area. Principal component 5: 255.20, 227.1, 277.19, 279.22, 283.26, 368.06, 687.49, 726.43, 740.55 are in the green area while 253.22, 281.21, 221.04, 296.79, 807.47, 833.50 are in the red area. Scale bar is 200 μm.

(C12:0), (C16:0), and (C16:1) at m/z 253.22 localize in the proboscis. Fatty acid (18:1), (C18:3), (C18:2), (18:0) at m/z 283.22, lipids PE (36:3) at m/z 740.55, PI (36:4) at m/z 857.55 and unknown species at m/z 260.86, 687.49, 659.43, 726.50 localize in the central brain; however, the distribution of those peaks seems to expand to a larger area in the MPH-treated brain compared to control brain. Furthermore, from the result of principal component 5, fatty acid (C14:0), (C16:0), (C18:3), (C18:2), (C18:0), lipid PE (36:3) and unknown species at m/z 687.49, 726.50 localize intensely across the entire control brain, whereas fatty acid (C16:1), (C18:1), PI (32:1) at m/z 807.47, PI (34:2) at m/z 833.50, and unknowns at m/z 221.04, 296.79 are found at higher intensity across the MPH-treated brain.

The data in both positive and negative modes have also been further examined in three narrower mass ranges in order to observe more detail in the distributional changes within specific chemical groups: m/z 180−450 for small mass molecules and fatty acids, m/z 450−600 for DAGs, and m/z 600−950 for intact lipids such as PCs, PEs, and PIs (Figure S3 in the Supporting Information). The results show that many biomolecules have various distributional patterns in the fly brain and they localize differently in the control and methylphenidate brains.

From the image PCA data, different principal components effectively highlight the relation of biomolecules regarding their spatial localizations and relative concentrations in the control and MPH-treated fly brains. From the PCA it is apparent that biomolecules significantly affected by the drug can be easily identified. This provides a qualitative overview of the biologically structural changes of the fly brain following the effects of methylphenidate. Significant peaks were then inspected for a relative quantitative comparison of the peak intensities in the next section.

Differences of Fly Brain Composition Caused by Methylphenidate. In order to observe in more detail how the biomolecules change between the control and MPH treated brains, all the peak intensities in the whole mass range were compared. Two regions of interest, the central brain and the optical lobes in each fly brain, were selected and the peak intensities in the spectra for each region were compared between the control and MPH brains. There are no significant changes in chemical composition in the optical lobes; however, remarkable differences are observed in the central brain between MPH treated and control brains. Figure 4 shows biomolecular differences in both positive and negative ion modes in the central brain of *Drosophila* exposed to methylphenidate.

In positive mode, several relatively low mass species are found to decrease in concentration in the central brain following MPH. The intensities of the peaks at m/z 255.01 and 504.37 decrease by approximately 25−30% compared to those in the control. The phosphatidylcholine headgroup intensity at m/z 184.07 in MPH treated brains also dropped by around 30%. On the other hand, there was a 2- to 4-fold increase in the amount of DAGs in the MPH treated brain such as DAG (30:1), DAG (32:1), DAG (32:2) at m/z 547.46 and DAG (34:2) at m/z 575.52. In contrast to the DAGs, the concentrations of intact lipids and their salt adducts decrease in the MPH brain, which is consistent with the decrease in the phosphatidylcholine headgroup intensity in MPH brains, particularly the amount of PC (34:1) and its salt adduct [PC (34:1) + K]$^+$ at m/z 798.56, which are about 30% lower than those of the control. PC (36:3) at m/z 784.60, PC (36:2) at m/z 786.63, and their salt adducts [PC (36:3) + K]$^+$ at m/z 822.55, [PC (36:2) + K]$^+$ at m/z 824.57 follow a similar tendency; however, to a lower extent. In addition, the unknown species at m/z 587.57, 766.63 are 50% in intensity following MPH compared to the control. The results are statistically significant according to the t test, and the p values vary between 0.003 and 0.049 (all with 95% confidence interval), except for DAG (30:1) and PC (36:3), which have p values between 0.050 and 0.100.

In negative ion mode, the biomolecular difference between the central brains of the control and MPH treated groups is not as significant as observed in positive ion mode. Most of the species show a slight increase in signal in the MPH-treated
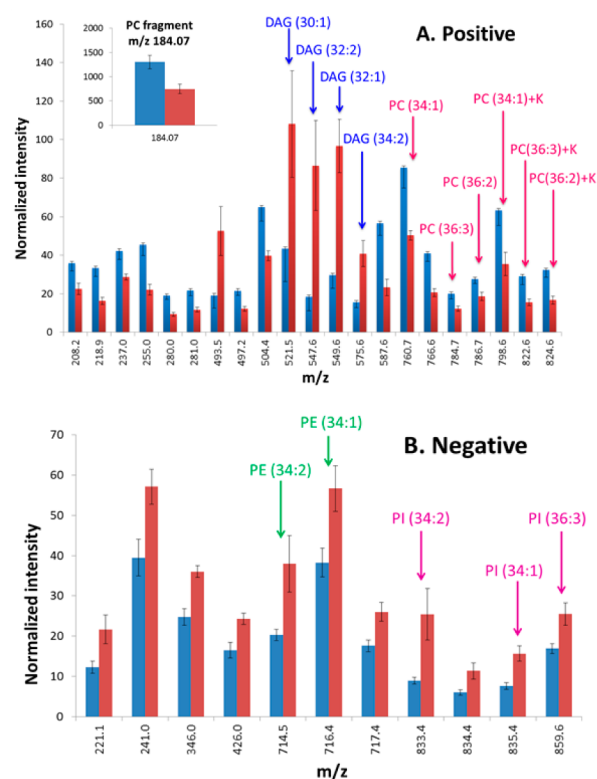

Figure 4. Relative quantification of biomolecular changes in the central brain of *Drosophila* following oral administration of methylphenidate in positive mode analyzed by 40 keV Ar$_{4000}$ GCIB. Comparison of 6 control brains (blue bars) and 4 MPH-treated brains (red bars). Peak intensities were normalized to the number of pixels and sum of all selected peaks obtained from image PCA. The error bar is the standard error of the mean. (A) Positive ion mode and (B) negative ion mode.

brains compared to the control. Several phosphatidylethanolamine (PE) and phosphatitylinositol (PI) lipids show a remarkable increase in the drug treated brain, particularly the peak intensities of PE (34:2) at m/z 714.36, PE (34:1) at m/z 716.34, and PI (32:1) increase about 1.3−2-fold; PI (34:2) is elevated about 3-fold. PI (36:3) and PI (34:1) at m/z 835.50, however, only increase slightly in the drug-treated brains. The data are statistically significant according to t test and the p values vary between 0.004 and 0.039 with a 95% confidence interval.

As mentioned above, MPH is a stimulant drug that increases the extracellular levels of neurotransmitters such as dopamine and serotonin by blocking the reuptake of the neurotransmitters by their transporters. The elevated monoamines in turn activate a variety of postsynaptic receptors to trigger cellular signaling transduction. It has been shown that phospholipid metabolic enzyme phospholipase A2 (PLA-2) is involved in the development of sensitization in rats treated with psychostimulants such as cocaine or amphetamine,[47] and there is a link between dopamine receptors D1, D2 and enzyme PLA-2.[48,49] Metabolism of membrane phospholipids occurs in the presence of a group of phospholipases mainly including phospholipase A1 (PLA-1), phospholipase A2 (PLA-2), phospholipase C (PLC), and phospholipase D (PLD); each has different sites of action on the glycerophospholipid molecules. PLA-2, comprising of Ca^{2+} dependent (Ca-PLA-2) and Ca^{2+} independent (PLA-2), relates to the hydrolysis of phosphatidylcholines and phosphatidylethanolamines as the
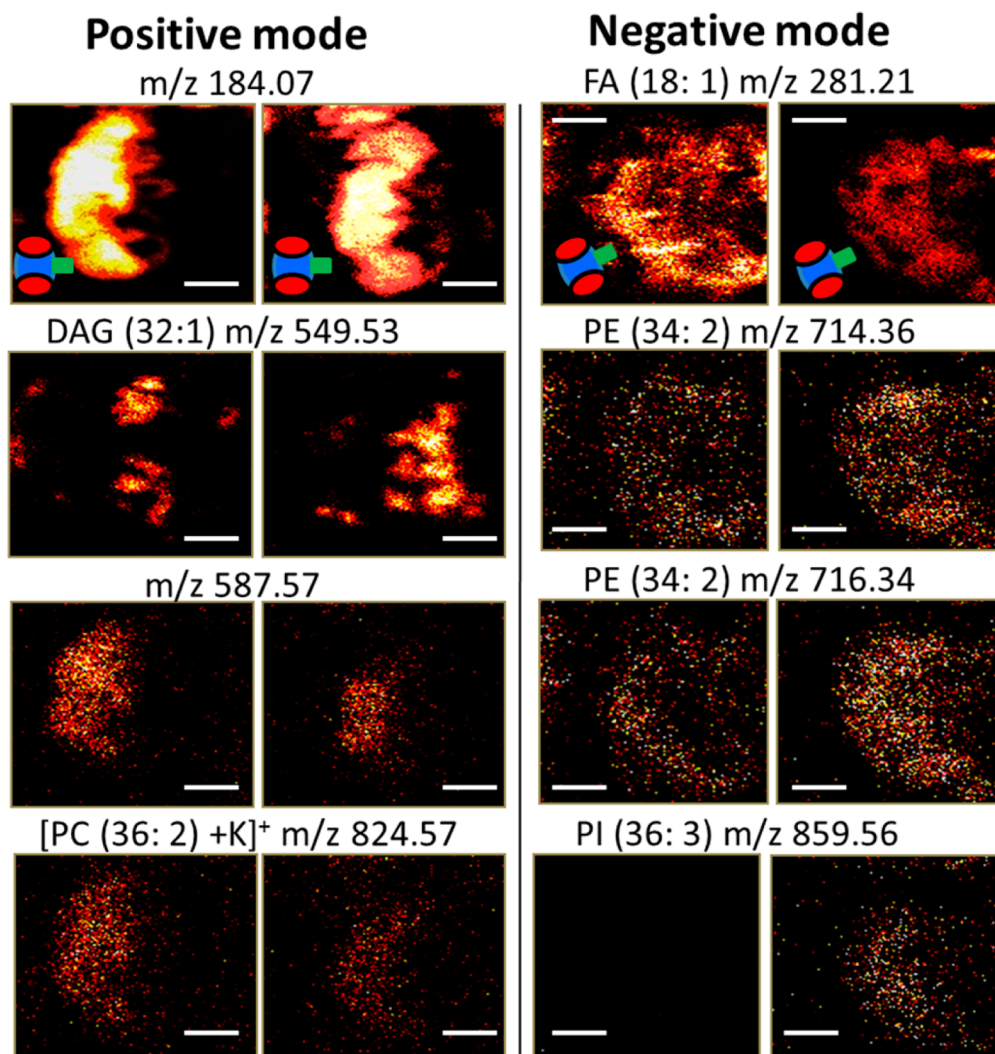
Figure 5. SIMS images of lipids across fly brains without and with methylphenidate administration. Left, control brains; right, MPH-treated brains. The symbolic figure shows orientation of the fly brains. Scale bar is 200 μm.

typical substrates.[31] The enzyme hydrolyzes the sn-2 ester bond of the glycerophospholipids to release fatty acid, typically arachidonic acid and 1-acyl lysophospholipid.[50] Arachidonic acid is an important secondary messenger that modulates Ca^{2+} ion channels, activities of protein kinase C, and monoamine transporters by inhibiting glutamate uptake. It has been found that the activity of Ca-PLA-2 is decreased in the dopamine-rich brain areas of cocaine and methamphetamine users.[51] The mechanism of the inhibitory effect is not fully understood. However, other findings suggested that the level of arachidonic acid is elevated with stimulant effects via activation of excitatory amino acid receptors such as glutamate receptors, N-methyl-D-aspartate (NMDA) receptors.[52−54] These findings appear contradictory because arachidonic acid is the typical metabolic product of glycerophospholipids hydrolyzed by PLA-2. According to Schinelli,[55] arachidonic acid levels might be modulated by dopamine receptor D1 in the striatal neurons, and the activity of the receptor can be regulated via the cyclic AMP pathway. PLA-2 activity might be also regulated by inhibitory G proteins.[56] Thus, it is possible that one action of stimulant drugs like cocaine, methamphetamine, and MPH is to increase arachidonic acid levels by the activation of dopamine receptors, and this could also send feedback to inhibit PLA-2

activity. The reduced activity of PLA-2 in the brain could therefore lead to the increased amount of its primary substrates, particularly PCs and PEs. However, the amount of glycerophospholipids is not only dependent on the metabolic but also influenced by their biosynthesis pathways. In addition to the activity of PLA-2 decreasing in stimulant drug users, Ross et al.[51] also found significantly reduced activity of phosphocholine cytidylyltransferase (PCCT), the rate limiting enzyme of PC-lipid synthesis. The reduced activity of this enzyme led to reduced levels of synthesized PCs in the brain. The inhibited activities of PLA-2 and PCCT could provide an explanation for our data in which PCs and their salt adduct concentrations decrease, whereas the PE levels increase in the MPH-treated fly brains.

The elevated arachidonic acid from stimulant administration also enhances the activity of PLD. This enzyme catalyzes the cleavage of glycerophospholipids, typically PCs, into phosphatidic acid and a free base.[31] Another pathway that could increase PLD activity might involve dopamine receptors or metabotropic glutamate receptors, which have been shown to directly affect amygdala PLD activity.[57] The increased PLD activity following a stimulant drug is also consistent with the

decreased concentration of PCs in MPH-treated fly brains observed in our data.

An explanation of the changes of PI levels in the drug-treated brain can be found by considering PLC. The metabolic enzyme hydrolyses the sn-3 phosphodiester bond of the PIs and their phosphorylated forms to release diacylglycerol and noncyclic or cyclic inositol phosphates.[31] The isoform PLC-B, a group of phosphoinositide specific enzymes coupled to guanine-nucleotides-G proteins, were found in *Drosophila* heads.[58] The activity of the PLC enzyme can apparently be altered by the effects of psychostimulants such as cocaine and amphetamine via the activation of metabotropic glutamate receptors,[59] possibly leading to an increase in the levels of phosphatidylinositols in MPH-treated fly brains.

The reason for the significant increase of DAGs in the MPH-treated brain is not clear; however, it is possible that the combination of the altered activities of different enzymes, especially PLC and PLD, or the elevated amount of TAGs in salivary gland lead to an increase in the DAG concentration.

Lipid Distribution of Fly Brain Following Methylphenidate Treatment. To verify the correlation of the results from image PCA and peak intensity comparison, the TOF-SIMS ion images of significant biomolecules of the control and MPH treated brains were examined. Figure 5 compares the ion images of different lipids across the fly brains following exposure to methylphenidate. The phosphatidylcholine head-group ion at m/z 184.07 is uniformly distributed across the whole brain section in both control and drug-treated groups; however, other species exhibit very different localization. Significant changes were observed in both positive and negative modes. In positive ion mode the DAGs, for instance DAG (32:1), mainly localize in the proboscis and salivary gland areas. The distributions of these molecules are slightly different between MPH-treated and control brains owing to easy delocalization in the proboscis during sectioning. In addition, the DAGs localize in the MPH-treated brain more intensely. The unknown peak at m/z 587.57 localizes in the central brain and optical lobes of the control brain, whereas it is only distributed in the central brain of the MPH-treated brain. We carried out MS/MS on this peak but have not yet concluded its structure. The PC salt adduct $[PC\ (36:3) + K]^+$ is mainly in the central brain at higher intensity in the control fly brain. In negative ion mode, fatty acid (18:1) is observed to distribute in the central brain but at lower intensity in MPH-treated brains. PE (34:2) and PE (34:1) localize in the whole brain area, however, at higher concentration in MPH-treated brains. Finally, PI (36:3) at m/z 859.56 mainly localizes in the MPH-treated central brain but is hardly observed in the control. Distributional information on other significant biomolecules of the drug treated and control brains are presented in Figures S4 and S5 in the Supporting Information.

The results obtained from image PCA, peak intensity comparison, and TOF-SIMS images are consistent. Combination of all these data analysis methods is very useful for mass spectrometric imaging in biological applications, allowing us to thoroughly examine and interpret huge and complex data with high reliability. It is clearly shown that methylphenidate affects the chemical structure of the fly brain. With the help of SIMS and SEM imaging together with image PCA for data analysis, the nervous system of the fly brain following drug administration can be visualized.

CONCLUSIONS

TOF-SIMS imaging has been successfully applied for the study of chemical structure in the fly brain following the administration of the stimulant drug methylphenidate. The use of the Ar_{4000} GCIB provides a tremendous advantage for the detection of various types of intact lipids (PCs, PEs, PIs, etc.) while the sensitivity of small species is unaffected. First, this improvement shows that the high energy Ar GCIB 40 keV is well suited for lipid imaging in biological areas. The chemical structure of the fly brain can be imaged with relatively high spatial resolution (3 μm/pixel). Second, correlation of SIMS and SEM imaging shows the apparent relation between the distribution and biological functions of different biomolecules in the fly brain. Third, data interpretation using image PCA, peak intensity comparison, and SIMS ion images shows that methylphenidate has significant actions on a variety of biomolecules, especially the elevated amount of DAGs, PEs, and PIs and a significant decrease of PC levels. Not only were their abundances changed but also their localizations in the brain varied. This alteration of brain lipid structure can cause serious damage to the function of the nervous system. TOF-SIMS imaging with the high energy Ar GCIB is a useful tool to examine the impact of methylphenidate on the fly brain.

ASSOCIATED CONTENT

⑤ Supporting Information

Figures demonstrating overlaid images of SIMS and SEM of a fly brain, the accumulated percentage of explained contribution by different principal components for image PCA within the mass range m/z 184−950, image PCA of molecular distribution on MPH treated and control fly brains in positive and negative ion modes, and SIMS ion images of different biomolecular species across the fly brains with and without MPH treatment in positive and negative modes. This material is available free of charge via the Internet at http://pubs.acs.org.

AUTHOR INFORMATION

Corresponding Author
*E-mail: andrew.ewing@chem.gu.se.

Notes
The authors declare no competing financial interest.

ACKNOWLEDGMENTS

REFERENCES

(1) Winhusen, T.; Somoza, E.; Singal, B. M.; Harrer, J.; Apparaju, S.; Mezinskis, J.; Desai, P.; Elkashef, A.; Chiang, C. N.; Horn, P. *Pharmacol., Biochem., Behav.* **2006**, *85*, 29−38.
(2) Kuczenski, R.; Segal, D. S. *J. Neurochem.* **1997**, *68*, 2032−2037.
(3) Phan, N. T.; Hanrieder, J.; Berglund, E. C.; Ewing, A. G. *Anal. Chem.* **2013**, *85*, 8448−8454.
(4) Schmitz, F.; Scherer, E. B.; Machado, F. R.; da Cunha, A. A.; Tagliari, B.; Netto, C. A.; Wyse, A. T. *Metabol. Brain Dis.* **2012**, *27*, 605−612.
(5) Charach, G.; Kaysar, N.; Rabinovich, A.; Argov, O.; Weintraub, M. Methylphenidate and Dyslipidemia. In *Current Directions in ADHD and Its Treatment*; InTech: New York, 2012; pp 185−192.
(6) Charach, G.; Kaysar, N.; Grosskopf, I.; Rabinovich, A.; Weintraub, M. *J. Clin. Pharmacol.* **2009**, *49*, 848−851.

(7) Pandey, U. B.; Nichols, C. D. *Pharmacol. Rev.* **2011**, *63*, 411−436.

(8) Wolf, F. W.; Heberlein, U. *J. Neurobiol.* **2003**, *54*, 161−178.

(9) Kraut, R. *J. Neurochem.* **2011**, *116*, 764−778.

(10) Kliman, M.; Vijayakrishnan, N.; Wang, L.; Tapp, J. T.; Broadie, K.; McLean, J. A. *Mol. BioSyst.* **2010**, *6*, 958−966.

(11) Berglund, E. C.; Makos, M. A.; Keighron, J. D.; Phan, N.; Heien, M. L.; Ewing, A. G. *ACS Chem. Neurosci.* **2013**, *4*, 566−574.

(12) Xun, Z.; Sowell, R. A.; Kaufman, T. C.; Clemmer, D. E. *J. Proteome Res.* **2007**, *6*, 3729−3738.

(13) Niehoff, A. C.; Kettling, H.; Pirkl, A.; Chiang, Y. N.; Dreisewerd, K.; Yew, J. Y. *Anal. Chem.* **2014**, *86*, 11086−11092.

(14) Urban, P. L.; Chang, C. H.; Wu, J. T.; Chen, Y. C. *Anal. Chem.* **2011**, *83*, 3918−3925.

(15) Phan, N. T. N.; Fletcher, J. S.; Sjövall, P.; Ewing, A. G. *Surf. Interface Anal.* **2014**, *46*, 123−126.

(16) Kotter, F.; Benninghoven, A. *Appl. Surf. Sci.* **1998**, *133*, 47−57.

(17) Kollmer, F. *Appl. Surf. Sci.* **2004**, *231−232*, 153−158.

(18) Touboul, D.; Kollmer, F.; Niehuis, E.; Brunelle, A.; Laprevote, O. *J. Am. Soc. Mass Spectrom.* **2005**, *16*, 1608−1618.

(19) Weibel, D.; Wong, S.; Lockyer, N.; Blenkinsopp, P.; Hill, R.; Vickerman, J. C. *Anal. Chem.* **2003**, *75*, 1754−1764.

(20) Ninomiya, S.; Ichiki, K.; Yamada, H.; Nakata, Y.; Seki, T.; Aoki, T.; Matsuo, J. *Rapid Commun. Mass Spectrom.* **2009**, *23*, 1601−1606.

(21) Bich, C.; Havelund, R.; Moellers, R.; Touboul, D.; Kollmer, F.; Niehuis, E.; Gilmore, I. S.; Brunelle, A. *Anal. Chem.* **2013**, *85*, 7745−7752.

(22) Sheraz nee Rabbani, S.; Barber, A.; Fletcher, J. S.; Lockyer, N. P.; Vickerman, J. C. *Anal. Chem.* **2013**, *85*, 5654−5658.

(23) Angerer, T. B.; Blenkinsopp, P.; Fletcher, J. S. *Int. J. Mass Spectrom.* **2015**, *377*, 591−598.

(24) Kuklinski, N. J.; Berglund, E. C.; Engelbrektsson, J.; Ewing, A. E. *Anal. Chem.* **2010**, *82*, 7729−7735.

(25) Fletcher, J. F.; Rabbani, S.; Henderson, A.; Blenkinsopp, P.; Thompson, S. P.; Lockyer, n. P.; Vickerman, J. C. *Anal. Chem.* **2008**, *80*, 9058−9064.

(26) Hill, R.; Blenkinsopp, P.; Thompson, S.; Vickerman, J.; Fletcher, J. S. *Surf. Interface Anal.* **2011**, *43*, 506−509.

(27) Allen, J. A.; Halverson-Tamboli, R. A.; Rasenick, M. M. *Nat. Rev. Neurosci.* **2007**, *8*, 128−140.

(28) Cooper, G. M. *The Cell: A Molecular Approach*, 2nd ed.; ASM Press: Washington, DC, 2000.

(29) Betterman, J. M.; Duronio, V.; Cuatrecasas, P. *Proc. Natl. Acad. Sci. U.S.A.* **1986**, *83*, 6785−6789.

(30) Cui, Z.; Houweling, M. *Biochim. Biophys. Acta* **2002**, *1585*, 87−96.

(31) Farooqui, A. A.; Horrocks, L. A.; Farooqui, T. *Chem. Phys. Lipids* **2000**, *106*, 1−29.

(32) Adibhatla, R. M.; Hatcher, J. F. *Future Lipidol.* **2007**, *2*, 403−422.

(33) Kaddurah-Daouk, R.; McEvoy, J.; Baillie, R.; Zhu, H.; J, K. Y.; Nimgaonkar, V. L.; Buckley, P. F.; Keshavan, M. S.; Georgiades, A.; Nasrallah, H. A. *Psychiatry Res.* **2012**, *198*, 347−352.

(34) Sugiura, Y.; Konishi, Y.; Zaima, N.; Kajihara, S.; Nakanishi, H.; Taguchi, R.; Setou, M. *J. Lipid Res.* **2009**, *50*, 1776−1788.

(35) Stubbs, C. D.; Smith, A. D. *Biochim. Biophys. Acta* **1984**, *779*, 89−137.

(36) Mikawa, S.; Suzuki, M.; Fujimoto, C.; Sato, K. *Neurosci. Lett.* **2009**, *451*, 45−49.

(37) Carter, C. L.; McLeod, C. W.; Bunch, J. *J. Am. Soc. Mass Spectrom.* **2011**, *22*, 1991−1998.

(38) Yew, J. Y.; Soltwisch, J.; Pirkl, A.; Dreisewerd, K. *J. Am. Soc. Mass Spectrom.* **2011**, *22*, 1273−1284.

(39) Gibbs, A. G. *Am. Zool.* **1998**, *38*, 471−482.

(40) Yeagle, P. L. *FASEB J.* **1989**, *3*, 1833−1842.

(41) Vance, J. E.; Tasseva, G. *Biochim. Biophys. Acta* **2013**, *1831*, 543−554.

(42) Janmey, P. A. *Chem. Biol.* **1995**, *2*, 61−65.

(43) Sjovall, P.; Lausmaa, J.; Johansson, B. *Anal. Chem.* **2004**, *76*, 4271−4278.

(44) Wang, H. Y.; Jackson, S. N.; Post, J.; Woods, A. S. *Int. J. Mass Spectrom.* **2008**, *278*, 143−149.

(45) Graham, D. J.; Wagner, M. S.; Castner, D. G. *Appl. Surf. Sci.* **2006**, *252*, 6860−6868.

(46) Fletcher, J. S.; Rabbani, S.; Henderson, A.; Lockyer, N. P.; Vickerman, J. C. *Rapid Commun. Mass Spectrom.* **2011**, *25*, 925−932.

(47) Reid, M. S.; Hsu, K.; Tolliver, B. K.; Crawford, C. A.; Berger, S. P. *J. Pharmacol. Exp. Ther.* **1996**, *276*, 1244−1256.

(48) Hussain, T.; Lokhandwala, M. F. *Clin. Exp. Hypertens.* **1997**, *19*, 131−140.

(49) Piomelli, D. *J. Neurochem.* **1995**, *64*, 2765−2772.

(50) Farooqui, A. A.; Ong, W. Y.; Horrocks, L. A. *Neurochem. Res.* **2004**, *29*, 1961−1977.

(51) Ross, B. M.; Moszczynska, A.; Peretti, F. J.; Adams, V.; Schmunkd, G. A.; Kalasinsky, K. S.; Ang, L.; Mamalias, N.; Turenne, S. D.; Kish, S. J. *Drug Alcohol Depend.* **2002**, *67*, 73−79.

(52) Fitzgerald, L. W.; Ortiz, J.; Hamedani, A. G.; Nestler, E. J. *J. Neurosci.* **1996**, *16*, 274−282.

(53) Swanson, C. J.; Baker, D. A.; Carson, D.; Worley, P. F.; Kalivas, P. W. *J. Neurosci.* **2001**, *21*, 9043−9052.

(54) Farooqui, A. A.; Horrocks, L. A. *Brain Res. Rev.* **1991**, *16*, 171−191.

(55) Schinelli, S. *J. Neurochem.* **1994**, *62*, 944−949.

(56) Felder, C. C.; Williams, H. L.; Axelrod, J. *Proc. Natl. Acad. Sci. U.S.A.* **1991**, *88*, 6477−6480.

(57) Krishnan, B.; Genzer, K. M.; Pollandt, S. W.; Liu, J.; Gallagher, J. P.; Shinnick-Gallagher, P. *PLoS One* **2011**, *6*, e25639.

(58) Bloomquist, B. T.; Shortridge, R. D.; Schneuwly, S.; Perdew, M.; Montell, C.; Steller, H.; Rubin, G.; Pak, W. L. *Cell* **1988**, *54*, 723−733.

(59) Byrnes, K. R.; Loane, D. J.; Faden, A. I. *J. Am. Soc. Exp. Neurother.* **2009**, *6*, 94−107.